NANO · MICRO small
www.small-journal.com

Check for updates

Volume-Enhanced Raman Scattering Detection of Viruses

Xingang Zhang, Xiaolei Zhang, Changliang Luo, Zhengqi Liu, Yiyun Chen, Shilian Dong, Changzhong Jiang, Shikuan Yang, Fubing Wang,* and Xiangheng Xiao**

Virus detection and analysis are of critical importance in biological fields and medicine. Surface-enhanced Raman scattering (SERS) has shown great promise in small molecule and even single molecule detection, and can provide fingerprint signals of molecules. Despite the powerful detection capabilities of SERS, the size discrepancy between the SERS "hot spots" (generally, <10 nm) and viruses (usually, sub-100 nm) yields poor detection reliability of viruses. Inspired by the concept of molecular imprinting, a volume-enhanced Raman scattering (VERS) substrate composed of hollow nanocones at the bottom of microbowls (HNCMB) is developed. The hollow nanocones of the resulting VERS substrates serve a twofold purpose: 1) extending the region of Raman signal enhancement from the nanocone surface (e.g., surface "hot spots") to the hollow area within the cone (e.g., volume "hot spots")—a novel method of Raman signal enhancement, and 2) directing analyte such as viruses of a wide range of sizes to those VERS "hot spots" while simultaneously increasing the surface area contributing to SERS. Using HNCMB VERS substrates, greatly improved Raman signals of single viruses are demonstrated, an achievement with important implications in disease diagnostics and monitoring, biomedical fields, as well as in clinical treatment.

1. Introduction

Viruses can cause an array of serious diseases, such as acquired immune deficiency syndrome or AIDS and Ebola virus caused Ebola hemorrhagic fever or EBHF. Adenoviruses can cause a wide range of clinical syndromes including hepatitis, upper respiratory tract infection, and pneumonia.[1] They also contain powerful oncogenes, which can promote tumor growth.[2] Because viruses can cause many serious illnesses, sensitive detection and accurate identification of viruses are crucial for disease monitoring and clinical treatment. Existing technologies such as fluorescent antibody assays,[3] enzyme-linked immunosorbent assay (ELISA),[4,5] and polymerase chain reaction (PCR)[6–8] were developed for the detection and analysis of viruses, but most of these technologies suffer from complex procedures, poor sensitivity, as well as time and cost ineffectiveness. Due to the lack of rapid and sensitive detection methods, the study of respiratory syncytial virus and the diagnosis of acute infection in adults have been seriously hindered.[9] Developing simple, fast, and economical virus detection techniques can allow for early viral infections identification, a crucial component of early treatment and increased likelihood of patient survival.[10]

One technology with powerful detection capabilities is surface-enhanced Raman scattering (SERS), which can detect small molecules at a single molecule level without complex sample treatment procedures.[11–14] SERS signals provide fingerprint signals unique to the molecular composition of the analyte, allowing for analyte identification.[15–17] More importantly, SERS is biocompatible because water—the main component of biofluids—is SERS inactive.[18–26] However, SERS is ineffective in reliably detecting and identifying viruses due to the size discrepancies between the SERS sensitive sites (known as "hot spots") and the viruses. SERS "hot spots" (i.e., regions where Raman signal is magnified by the resonance of local electrons within the substrate) usually exist between adjacent noble metal nanostructures placed <10 nm apart.[27–34] In contrast, viruses are usually several tens of nanometers and are composed of complex components (e.g., protein, DNA, RNA, etc.).[1,6,35–44] Due to these geometry constraints, most whole viruses cannot fit into SERS "hot spots." While virus surface deformation may enable part of their surfaces to penetrate into the SERS "hot spots," this reveals little about the virus as

Dr. X. G. Zhang, Dr. X. L. Zhang, Prof. Y. Chen, Dr. S. Dong, Prof. C. Jiang, Prof. X. Xiao
Department of Physics and Key Laboratory of Artificial Micro- and Nano-structures of Ministry of Education
Hubei Nuclear Solid Physics Key Laboratory and Center for Ion Beam Application
School of Resource and Environmental Science
Wuhan University
Wuhan 430072, China
E-mail: xxh@whu.edu.cn

Dr. C. Luo, Prof. F. Wang
Department of Clinical Laboratory Medicine and Center for Gene Diagnosis
Zhongnan Hospital of Wuhan University
Wuhan 430071, China
E-mail: wfb20042002@sina.com

Prof. Z. Liu
Institute of Optoelectronic Materials and Technology
College of Physics and Communication Electronics
Jiangxi Normal University
Nanchang 330022, China

Prof. S. Yang
Institute for Composites Science Innovation
School of Materials Science and Engineering
Zhejiang University
Hangzhou 310027, China
E-mail: shkyang@zju.edu.cn

The ORCID identification number(s) for the author(s) of this article can be found under https://doi.org/10.1002/smll.201805516.

DOI: 10.1002/smll.201805516

© 2019 WILEY-VCH Verlag GmbH & Co. KGaA, Weinheim

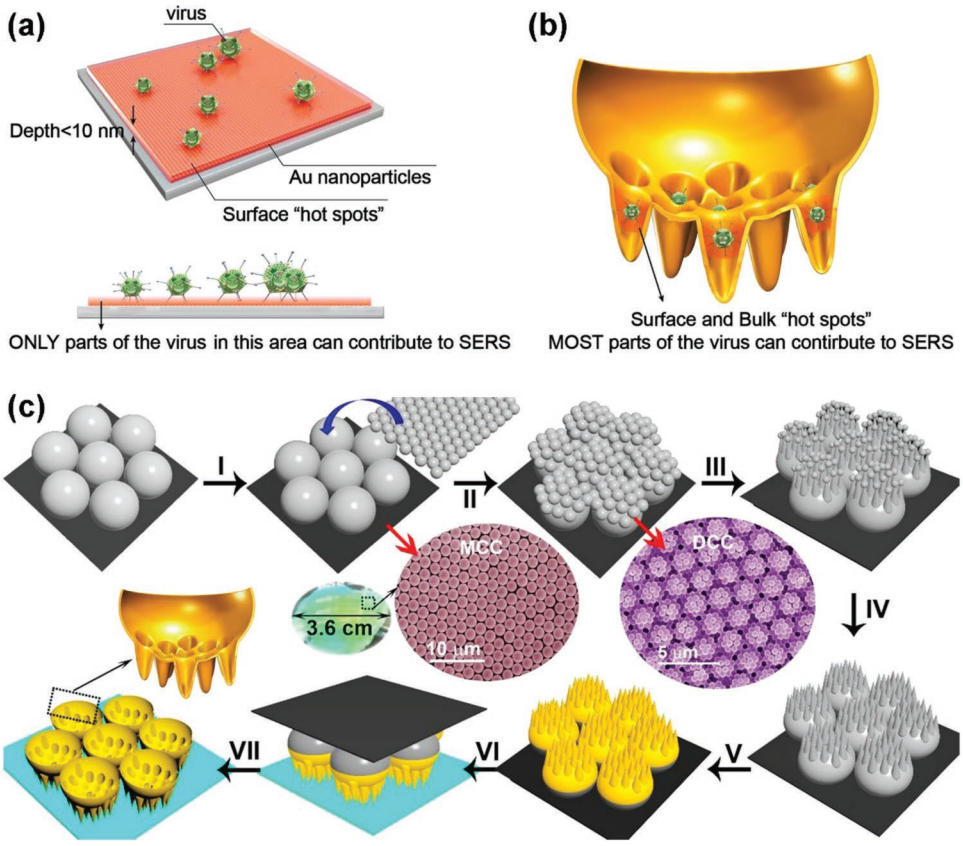

Figure 1. Concept of VERS detection of viruses. a) Conventional SERS substrates only collect the Raman signals from a small part of the virus. b) HNCMB structures enable most part of the virus to contribute to the Raman signals. Therefore, the Raman signals of single viruses on HNCMB structures are stronger and more comprehensive than those on conventional SERS substrates. c) Fabrication process of the gold HNCMB structures. Process I and II: Preparation of DCC template via stacking two MCC templates. Process III: Plasma etching of the DCC template for a short time. Process IV: Further plasma etching until the top small PS spheres are etched away. Process V: Evaporation a thin layer of gold film. Process VI: Inversion of the gold-coated plasma-etched DCC template. Process VII: HNCMB structures are obtained after removing PS sphere using dichloromethane. Insets show SEM images of the morphology of MCC (an optical image is also shown) and DCC structures, and an enlarged schematic of HNCMB structures.

a whole (**Figure 1**a). As a result, the captured SERS spectrum of the viruses using conventional SERS substrates has a poor signal reproducibility and thus poor detection reliability.[45–48] In an effort to achieve SERS-based virus detection, new strategies for collecting comprehensive SERS information of viruses are necessary.

Inspired by molecular imprinting, a concept that uses cavities to recognize molecules with the same geometry,[49,50] we developed a novel concept of volume-enhanced Raman scattering (VERS) and a substrate capable of achieving it with volumetric "hot spots." These hot spots were composed of hexagonally arranged hollow nanocones located at the bottom of the microbowls (referred as HNCMB structures) (Figure 1b). Unlike conventional SERS substrates[51,52] that only facilitate nanoscale surface "hot spots" (Figure 1a), HNCMB substrates exhibit strong electromagnetic fields not only at the surface, but also within the volume of the hollow nanocones, as revealed by finite-difference time-domain (FDTD) simulations. As a result, regions within the nanocones can behave as volume "hot spots" (Figure 1b). Most viruses are capable of physically fitting into the geometries of VERS hot spots, making it possible to acquire comprehensive Raman signals of the whole virus, significantly suppressing the virus orientation–induced irreproducibility of the Raman signals of conventional SERS substrates. Moreover, the contact area between the virus and the hollow nanocone is large than that between the virus and conventional SERS substrates. The increased contact area increased the portion of the virus surface area that can penetrate into the surface "hot spots." The hollow nanocones can be used to accommodate viruses in a wide size range, making them suitable for detecting several kinds of viruses with different sizes simultaneously.

Inspired by "molecular imprinting," this research effort introduced VERS and demonstrated that VERS substrates facilitate sensitive and reliable detection of viruses (Figure 1b). Experimentally, fingerprint Raman signals of adenovirus type 5 (Ad5) and coxsackievirus type 3 (Cv3) were observed using the HNCMB VERS substrates. HNCMB VERS substrates allow for significantly higher Raman signal reproducibility of Ad5 compared to conventional SERS substrates (here, a thermally evaporated gold film). VERS substrates can obtain comprehensive Raman peaks from single viruses and, in turn, achieve reliable identification of single viruses. Such VERS-enabled capabilities are of great potential in biology and biomedical fields.

© 2019 WILEY-VCH Verlag GmbH & Co. KGaA, Weinheim

2. Results and Discussion

2.1. Construction and Characterization of HNCMB SERS Sensors

The HNCMB VERS substrate was prepared in two steps (Figure 1c). First, a double-layer colloidal crystal (DCC) template was prepared by stacking a monolayer colloidal crystal (MCC) template composed of small polystyrene (PS) spheres onto another MCC template composed of large PS spheres (Process I and II in Figure 1c and Figure S1, Supporting Information).[53,54] The MCC template was prepared by a self-assembly process at the air/water interface.[55–57] Once the small PS spheres are applied to the large PS spheres to form the DCC template, the small PS spheres are approximately hexagonally closely packed on the large PS spheres (inset SEM image in Figure 1c and Figure S2, Supporting Information). These small PS spheres act as sacrificial dynamic protection templates during plasma etching treatment of the DCC template (Process III and IV in Figure 1c). As the small PS spheres are also subject to plasma etching, the area they can protect from being plasma etched gets smaller, giving rise to the formation of well-ordered PS nanocones standing on the large PS spheres (**Figure 2**a–h; Figure S3, Supporting Information). Second, a 100 nm thick gold film was thermally evaporated onto the plasma-treated DCC template (Process V in Figure 1c). After inverting the template using a method widely used to transfer graphene from one substrate to another[58] and removing the DCC template by immersion in dichloromethane, a HNCMB structure–formed ordered array was obtained (Process VI and VII in Figure 1c).

The length and the base diameter of the PS nanocones can be simply controlled by the plasma etching time and the diameter of the PS spheres chosen (Figure 2a–g and Figure S3, Supporting Information). The evolution of the length and the base diameter of the PS nanocones as plasma etching proceeds was carefully studied and is summarized in Figure 2h. We can design the height (h) of the PS nanocones using the following equation: $h = 4.88\ \text{nm min}^{-1} \times t$ where t is the plasma etching time. The width at the middle of the nanocones can be predicted by the following equation: $w = -2.24\ \text{nm min}^{-1} \times t + 287.12\ \text{nm}$. Therefore, the size and morphology of the PS nanocones can be accurately engineered.

The structural controllability of the PS nanocones allows us to design hollow nanocones that can accommodate viruses of different sizes. Viruses can be delivered into the hollow nanocone structures, where they are then tightly embedded. Considering that the size of the Ad5 virus is in the range of 60–90 nm,[1] we prepared HNCMB VERS substrate composed of microbowls with a diameter of ≈1.5 µm and nanocones with an opening size of ≈100 nm (Figure 2i–l), generated from gold replication of the plasma-etched DCC template composed of 2 µm PS spheres on the bottom and 290 nm PS spheres on top. Microscopic photos showed the highly ordered arrangement of these HNCMB structures (Figure S4, Supporting Information).

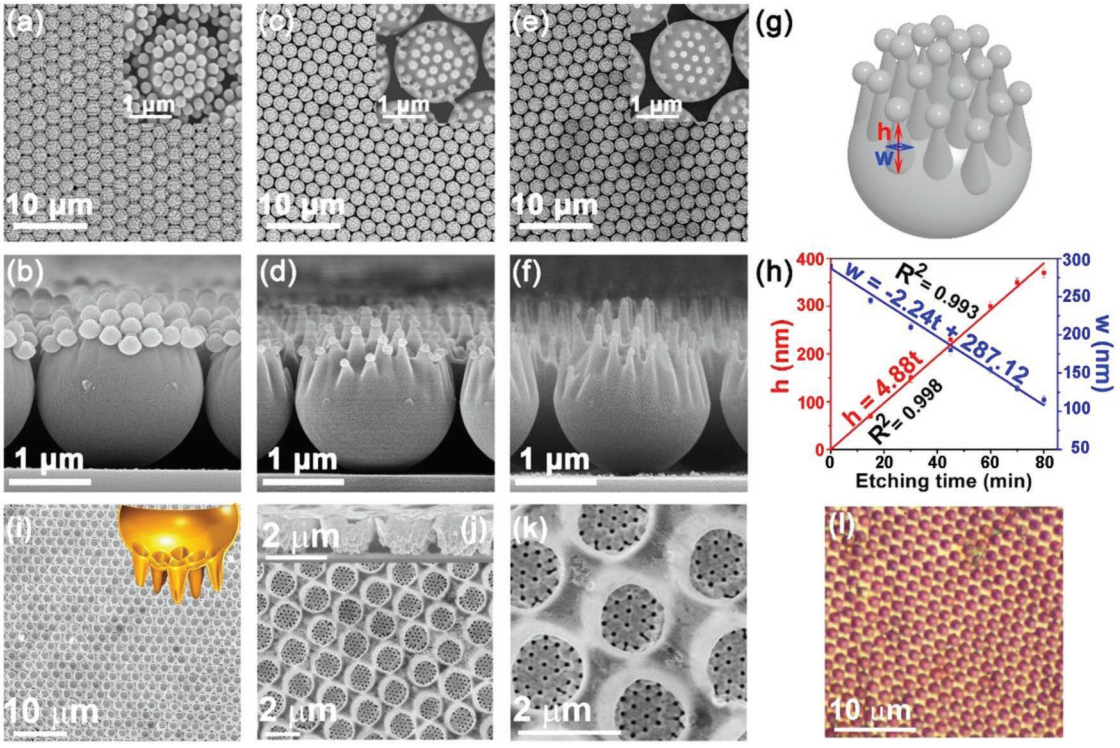

Figure 2. Characterization of the plasma-etched DCC template and the HNCMB structures. a,c,e) Top-view observation of the DCC template after plasma etching for 15, 45, and 70 min, respectively. b,d,f) The corresponding side-view image. g) Schematic of a plasma etched unit of the DCC template. h) The relationship between the width at the half length and the height of the cones to the plasma etching time. i) A large-area highly ordered HNCMB structure array. Inset in (i): schematic of a cross-sectional view of a HNCMB structure. j,k) Enlarged observation of the HNCMB structures. Inset in (j): side-view observation. The opening of the hollow nanocones can be observed in (j). l) A microscopic image of the HNCMB structure.

© 2019 WILEY-VCH Verlag GmbH & Co. KGaA, Weinheim

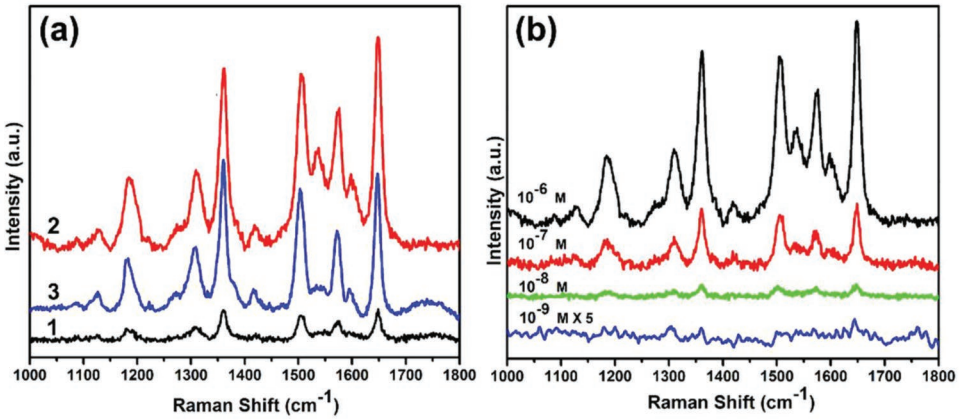

Figure 3. SERS performance of the HNCMB structures. a) Curve 1 and 2 are the SERS spectra of R6G molecules dissolved in water and ethanol at a concentration of 10^{-6} M on the as-prepared HNCMB structures, respectively. Curve 3 is the SERS spectrum of R6G molecules dissolved in water at a concentration of 10^{-6} M on the plasma-treated hydrophilic HNCMB structures. b) SERS spectra of R6G molecules dissolved in water at different concentrations on the plasma-treated hydrophilic HNCMB structures.

The roughness of the surface inside the hollow nanocones dictates the SERS performance of the substrate. This roughness is inherited from that of the plasma-treated PS surface, and was determined to be 5 nm ± 4.5 nm by atomic force measurements (Figure S5, Supporting Information). The SERS performance of the HNCMB was evaluated using Rhodamine 6G (R6G) as a probing molecule (**Figure 3**). The HNCMB SERS substrate was immersed into ethanol and aqueous solutions of R6G at different concentrations for 2 h. Then, the HNCMB structure was dried in ambient room conditions before SERS measurement. It was found that strong SERS signals of R6G molecules were observed from an ethanol solution of R6G at a concentration of 10^{-6} M. In contrast, the SERS signals from an aqueous solution of R6G were very weak. This is induced by the hydrophobic property of the HNCMB structure with a contact angle of about 106° (Figure S6, Supporting Information), which prohibits R6G molecules from entering the hollow nanocones. After plasma treatment, the HNCMB structure was rendered hydrophilic (i.e., with a water contact angle of about 35°), allowing water and thus the R6G molecules to enter the hollow nanocones. As a result, the SERS signals of R6G from aqueous solutions were significantly enhanced—the signal strengths using the plasma-treated HNCMB structures were comparable to those from ethanol solutions at the same concentrations. SERS signals of R6G were observable even at R6G concentrations as low as 10^{-8} M when using the plasma-treated HNCMB structures, and the detection limit is calculated to be 0.8×10^{-9} M according to the 3σ criterion, demonstrating outstanding SERS performance. Therefore, the HNCMB structure was plasma-treated to be hydrophilic before virus detection in all of the following experiments unless otherwise noted. No SERS peaks can be observed in pure water and ethanol (Figure S7, Supporting Information).

FDTD simulation results demonstrated that strong electromagnetic fields exist not only close to the inner surface of the hollow nanocones, but spread over the hollow area of the nanocones (**Figure 4**a). The HNCMB structure not only has "hot spots" tightly close to the surface (or surface "hot spots") but has

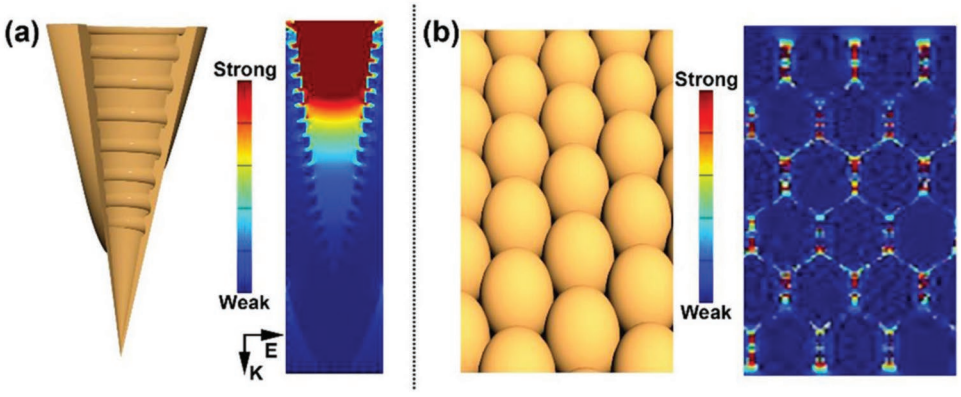

Figure 4. The distribution of the electromagnetic fields within different structures simulated by FDTD. a) Scheme of and the simulation result of the hollow nanocone. b) Scheme of and the simulation result of the gold nanoparticle film. The incident direction (K) and the polarization (E) of the 638 nm laser light are shown in (a). The hollow nanocone used for FDTD simulation was 360 nm in height with an opening size of 100 nm. The roughness of the hollow nanocone was reflected by the nanogrooves. The thermally evaporated gold film was represented as a monolayer of close-packed gold nanoparticles with a size of 100 nm.

© 2019 WILEY-VCH Verlag GmbH & Co. KGaA, Weinheim

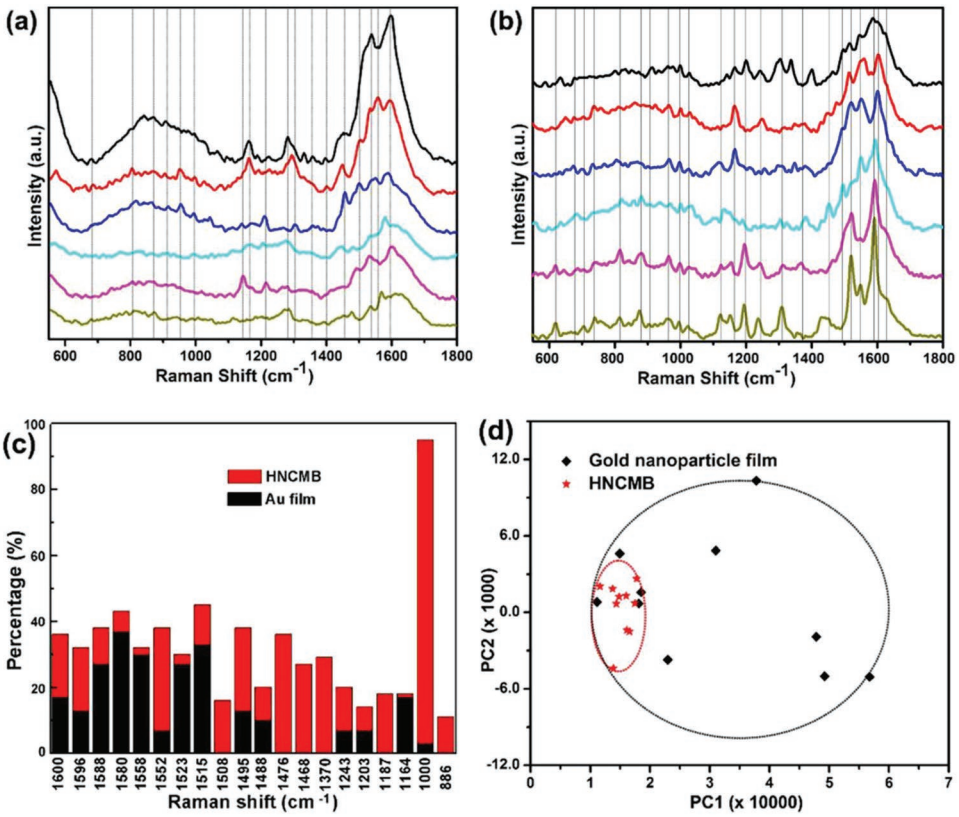

Figure 5. Detection of viruses using different sensing substrates. a,b) Six randomly chosen typical Raman spectra of single viruses dispersed on the gold nanoparticle film and on the HNCMB structures, respectively. c) The appearance rate of 20 randomly chosen Raman peaks of viruses on the gold nanoparticle film and the HNCMB structures. The appearance rate was calculated by counting the appearance times of a certain Raman peak in more than 50 SERS spectra of viruses. d) PCA plot of PC1 and PC2 computed from the Raman spectra of viruses obtained from the gold nanoparticle film and the HNCMB structure. A data point represents a Raman spectrum in the plot. The characteristic features of a Raman spectrum are reflected from the position of its corresponding point.

"hot spots" far away from the surface (or volume "hot spots"). Because the HNCMB structure allows for such volumetric Raman signal enhancement, we refer to it as a VERS substrate. The surface and volume "hot spots" can work together to sense analyte such as viruses, while conventional SERS substrates can only rely on surface "hot spots" (Figure 4b).

2.2. Detection of Ad5 with HNCMB VERS and Gold Film SERS Substrate

Experimentally, we compared the reproducibility of the Raman signals of Ad5 in a size range of 60–90 nm (Figure S8, Supporting Information) dispersed on the HNCMB VERS substrate with those dispersed on thermally evaporated gold film representing a conventional SERS substrate with only surface "hot spots." A piece of plasma-treated HNCMB structure (about 0.5 cm × 0.5 cm) was immersed into a cylindrical well filled with 200 µL of Ad5 dispersions with a concentration of 10^6 pfu mL^{-1}. The low concentration of the viruses ensures that at most one virus is trapped within each hollow nanocone. The microbowl structure facilitates delivery of viruses into the hollow nanocones. After sedimentation for 2 h, the 60–90 nm viruses are embedded in the hollow nanocones that have an opening size of ≈100 nm. The spot size of the laser is about 1.5 µm, which is the same size of the microbowls. While this size consistency assures that a single HNCMB structure can be used as a single-particle VERS substrate, a Raman signal may not be obtained at every microbowl at low analyte concentrations due to sparse virus distributions or poor virus embedding within the hollow nanocone. Under such conditions, we performed Raman mapping measurements over the HNCMB structure to address the location of the viruses (Figure S9, Supporting Information). Eventually, 56 and 30 Raman spectra of individual viruses were collected over the HNCMB VERS substrate and the thermally evaporated gold SERS substrate, respectively (Figures S10 and S11, Supporting Information). Generally, more Raman peaks appeared on the HNCMB VERS substrate than on the thermally evaporated gold film (**Figure 5**a,b). This means that the HNCMB VERS substrate can provide more comprehensive Raman information of a single virus than the thermally evaporated gold SERS substrate. The origin of these Raman peaks from the viruses is summarized in Table S1 in the Supporting Information. As aforementioned, different parts of the virus randomly penetrate into the surface "hot spots" of traditional SERS substrates exemplified by the thermally evaporated gold film (Figure 1). As a result, the SERS-based Raman peaks of the virus were limited and the Raman signals exhibited extremely

© 2019 WILEY-VCH Verlag GmbH & Co. KGaA, Weinheim

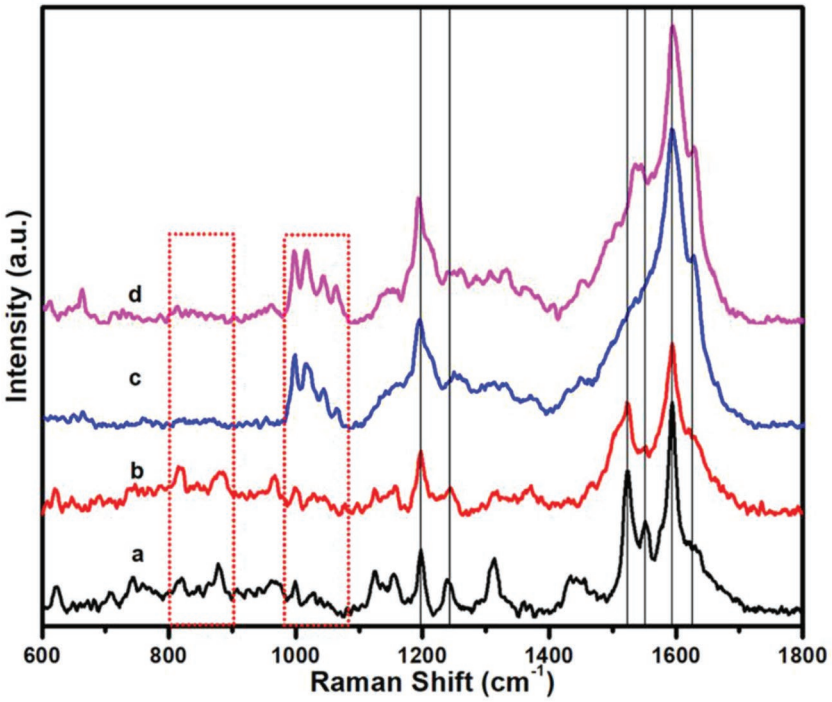

Figure 6. Typical Raman spectra of Ad5 (Curve a and b) and Cv3 (Curve c and d).

poor reproducibility (Figure 5a and Figure S11, Supporting Information). Comparatively, rich Raman signals of virus on the HNCMB VERS substrate were observed (Figure 5b and Figure S10, Supporting Information), because of the following two reasons: First, the interface area between the virus and the HNCMB VERS substrate is higher compared to that between the virus and the thermally evaporated gold film. Therefore, the probability of parts of a virus going into the surface "hot spots" is increased. Second, the volume "hot spots" within the hollow allow parts of the virus far away from the surface "hot spots" to contribute to the Raman signals (Figures 1 and 4).

To quantitatively evaluate the reproducibility of the Raman signals of viruses, we statistically calculated the appearance rate of certain Raman peaks from viruses as summarized in Table S1 in the Supporting Information. The appearance rate here represents the ratio of the number of times a peak appears to all the spectral numbers obtained on the same substrate. We randomly picked 20 Raman peaks from the virus on the thermally evaporated gold SERS substrate and the HNCMB VERS substrate and measured the appearance rate of the Raman peaks of interest (Figure 5c). Generally, the appearance rate of the Raman peaks of the virus is several times higher on the HNCMB VERS substrate than that on the thermally evaporated gold film. In other words, the signal reproducibility and in turn the detection reliability is greatly improved by using the "molecular imprinting"–inspired HNCMB VERS substrates composed of both surface and bulk "hot spots".

Principal component analysis (PCA) studies of the Raman spectra of viruses on different sensing substrates were further performed. PCA is a method which projects a data set into a transformed space that maximizes the variability within the data and thus allows spectral similarities and differences to be more easily observed. The points representing the Raman spectra obtained from the viruses on the HNCMB VERS substrate clustered more closely than those representing the Raman spectra of the viruses on the gold nanoparticle film. This shows that the HNCMB VERS substrate can provide more reproducible Raman spectrum of viruses than the gold nanoparticle film, indicating a good detection reliability of viruses using the HNCMB structures (Figure 5d).

To obtain comprehensive SERS signals of a certain virus, the size of the hollow nanocones should be judiciously designed. For example, the advantages of the hollow nanocones with an opening size of ≈100 nm are significantly weakened when they are used to detect Cv3 (with a concentration of 10^6 OPU mL^{-1}) with a size of around 25 nm (Figure S12, Supporting Information).[59] The origin of the Raman peaks from Cv3 is summarized in Table S2 in the Supporting Information. It was found that a good reproducibility of the Raman signals was observed on the thermally evaporated gold film, which is even better than that on the HNCMB VERS substrate (Figure S12, Supporting Information). This is because the size of the virus is close to the length that the SERS "hot spots" in the gold nanoparticle films can sense. Further considering the composition symmetry of the virus, it is not surprising that a good reproducibility of the SERS signals of Cv3 was observed on the thermally evaporated gold film. In contrast, the Cv3 will be delivered into the bottom part of the hollow nanocones where the electromagnetic field is weak (Figure 4a). Therefore, weak Raman signals of Cv3 with a poor signal reproducibility was observed on the HNCMB structures.

The Raman signals of Ad5 and Cv3 were compared (**Figure 6**). It was found that the main difference between the Raman spectra of the two viruses was in the wavenumber range between 800 and 1100 cm^{-1}. Specifically, two peaks located at 820 cm^{-1} (C–C str) and 879 cm^{-1} (Trp) were observed in the SERS spectra of Ad5 (Curve a and b in Figure 6), while absent in the SERS spectra of Cv3. Three peaks located at 1015 cm^{-1} (Carbohydrates peak for solids), and 1041 cm^{-1} (C–N str), and 1062 cm^{-1} (C–N str) appeared for Cv3, while absent in the SERS spectra of Ad5. The obvious difference of the SERS spectrum of different viruses makes virus identification possible, provided that comprehensive SERS signals of viruses could be collected employing the VERS technique.

3. Conclusions

Inspired by the "molecular imprinting" concept, we designed HNCMB VERS with not only surface "hot spots" close to the inner surface of the hollow nanocones, but volume "hot spots" far away from the surface, as verified by FDTD simulations. These VERS substrates allowed for large interfacial area between the virus and the inner surface of the hollow nanocone,

© 2019 WILEY-VCH Verlag GmbH & Co. KGaA, Weinheim

thus increasing the area of the virus that can contribute to the Raman signals, and also created volume "hot spots," which allowed for Raman information collection of the parts of the virus far away from the surface "hot spots." The reproducibility of the Raman signals and the detection reliability of single viruses are significantly improved using the "molecular imprinting"–inspired HNCMB VERS substrate. This study opens a new avenue toward engineering substrates that can collect comprehensive Raman signals of single viruses, which has crucial importance in disease diagnostics and biomedical fields.

4. Experimental Section

Preparation of the DCC Template: A piece of smooth copper foil (2×4 cm^2) was washed thoroughly with ethanol and deionized water and kept in 10 wt% sodium dodecyl sulfate (SDS) solutions for 12 h to obtain a highly hydrophilic surface. After flushing off the physically attached SDS with deionized water, the copper foil was dipped into deionized water at an angle of 80° to vertical. One hundred microliters of the PS sphere dispersions (about 2 wt%) in a mixture of water and ethanol at a volume ratio of 2:1 were dripped into water slowly along a glass slide. After introducing 100 µL of 5 wt% SDS solutions, the PS spheres assembled at the air/water interface to form an MCC template. After decanting the water slowly, the MCC template was transferred onto the copper foil. After drying naturally, the second layer MCC template was transferred onto the preformed MCC template using the same process as transferring the first layer MCC template, gaving rise to the formation of the DCC template (Figure S1, Supporting Information).

Preparation of the HNCMB Structures: The DCC template was etched by an oxygen plasma cleaner operated at a power of 30 W. The plasma etching time was varied from 0 to 90 min. The chamber pressure of the oxygen plasma cleaner was maintained at 10 Pa. Then, a layer of gold film with a thickness of 100 nm was thermally evaporated onto the plasma-treated DCC template. The gold-coated plasma-treated DCC template was put upside down on a piece of Si/SiO_2 wafer with the four sides being fixed by tape. An aqueous solution composed of iron chloride (17 wt%) and HCl (3 wt%) was slowly added onto the surface of the copper foil until the copper foil was completely covered by the etching solution. After 30 min, the copper foil was etched away, leaving behind the orientation-reversed gold-coated plasma-treated DCC template. Consequently, the orientation-reversed gold-coated plasma-etched DCC template was immersed in dichloromethane for 1 min to remove the PS spheres, leading to the formation of HNCMB structures.

Virus Treatment for SERS Analysis: The viruses (Ad5 and Cv3) were obtained from Zhongnan Hospital of Wuhan University, Wuhan, China. The viruses were stored at −20 °C before usage. The Ad5 titer of the original stocks was 10^{11} plaqueforming units (PFU) per mL while Cv3 was estimated to be $\approx 10^{11}$ optical particle unit (OPU) per mL. It was diluted by different times using the phosphate buffered saline (PBS) solutions for SERS analysis.

SERS and VERS Measurements: The SERS performance of the HNCMB structures and the gold nanoparticle film was performed on a confocal Raman instrument (RenishawinVia, Renishaw) using R6G as a probing molecule. The laser beam was focused onto the SERS substrate through a 100× objective. The laser power was about 60 µW. The integration time for SERS measurements was kept at 10 s. VERS measurement of the Ad5 and Cv3 virus were performed on a confocal Raman instrument (LabRAM HR Evolution) equipped with a 638 nm wavelength laser. A raster laser scan was carried out over the HNCMB structures and the gold nanoparticle film to obtain the VERS mapping results. The spot size of the laser beam was about 1.5 µm in diameter. The laser beam was focused through a 10× objective. The laser power was about 5 mW. The integration time was 15 s.

FDTD Simulation of the Electromagnetic Field Distribution over the SERS Substrates: The electromagnetic field distribution over the SERS substrates under 638 nm laser irradiation was simulated by the FDTD method. For simplification, the electromagnetic field distribution over the hollow nanocones used to trap and sense viruses was simulated. The simulation model of the hollow nanocones had an opening size of 100 nm and a height of 360 nm. The thermally evaporated gold film was simplified to be a layer of close-packed gold nanoparticles with a diameter of 100 nm. The K- and E-vectors corresponded to the incident direction of the laser light and the polarization direction, respectively. The optical parameters for gold were supplied by the FDTD software without modifications.

Supporting Information

Supporting Information is available from the Wiley Online Library or from the author.

Acknowledgements

X.G.Z., X.L.Z., and C.L. contributed equally to this work. The authors thank Dr. Birgitt B. Stogin of The Pennsylvania State University for the help in revising this article. The authors thank the Hongxing Xu Group of Wuhan University for the support of Raman spectrum measurements. The authors thank Dr. Yilin Lu and Mr. Weiyong Li from HORIBA China for technical support. The authors acknowledge the NSFC (51571153, 11722543, U1867215, 11875211), the Fundamental Research Funds for the Central Universities (2042017kf0168), Suzhou key industrial technology innovation project (SYG201828) for their funding support.

Conflict of Interest

The authors declare no conflict of interest.

Keywords

monolayer colloidal crystal, SERS, virus detection, volume-enhanced Raman scattering

Received: December 27, 2018
Revised: January 16, 2019
Published online:

[1] T. Lion, *Clin. Microbiol. Rev.* **2014**, *27*, 441.
[2] J. J. Trentin, Y. Yabe, G. Taylor, *Science* **1962**, *137*, 835.
[3] Y. L. Chenxiang Lin, Hao Yan, *Nano Lett.* **2007**, *7*, 507.
[4] Y. Q. Li, B. Zhu, Y. Li, W. R. Leow, R. Goh, B. Ma, E. Fong, M. Tang, X. Chen, *Angew. Chem., Int. Ed.* **2014**, *53*, 5837.
[5] A. A. Yanik, M. Huang, O. Kamohara, A. Artar, T. W. Geisbert, J. H. Connor, H. Altug, *Nano Lett.* **2010**, *10*, 4962.
[6] M. G. Ison, *Clin. Infect. Dis.* **2006**, *43*, 331.
[7] T. Lion, R. Baumgartinger, F. Watzinger, S. Matthes-Martin, M. Suda, S. Preuner, B. Futterknecht, A. Lawitschka, C. Peters, U. Potschger, H. Gadner, *Blood* **2003**, *102*, 1114.
[8] M. Echavarria, M. Forman, M. J. D. van Tol, J. M. Vossen, P. Charache, A. C. M. Kroes, *Lancet* **2001**, *358*, 384.
[9] M. K. O'Shea, M. A. Ryan, A. W. Hawksworth, B. J. Alsip, G. C. Gray, *Clin. Infect. Dis.* **2005**, *41*, 311.
[10] J.-H. Lee, B.-C. Kim, O. H. Byeung-Keun, J.-W. Choi, *J. Biomed. Nanotechnol.* **2015**, *11*, 2223.
[11] J. Kneipp, H. Kneipp, K. Kneipp, *Chem. Soc. Rev.* **2008**, *37*, 1052.
[12] X. M. Qian, S. M. Nie, *Chem. Soc. Rev.* **2008**, *37*, 912.

© 2019 WILEY-VCH Verlag GmbH & Co. KGaA, Weinheim

[13] H. Y. Chen, M. H. Lin, C. Y. Wang, Y. M. Chang, S. Gwo, *J. Am. Chem. Soc.* **2015**, *137*, 13698.
[14] A. B. Zrimsek, N. Chiang, M. Mattei, S. Zaleski, M. O. McAnally, C. T. Chapman, A. I. Henry, G. C. Schatz, R. P. Van Duyne, *Chem. Rev.* **2017**, *117*, 7583.
[15] Y. B. Zheng, J. L. Payton, C. H. Chung, R. Liu, S. Cheunkar, B. K. Pathem, Y. Yang, L. Jensen, P. S. Weiss, *Nano Lett.* **2011**, *11*, 3447.
[16] C. Zhu, G. Meng, P. Zheng, Q. Huang, Z. Li, X. Hu, X. Wang, Z. Huang, F. Li, N. Wu, *Adv. Mater.* **2016**, *28*, 4871.
[17] M. T. Sun, H. X. Xu, *Small* **2012**, *8*, 2777.
[18] S. K. Yang, X. M. Dai, B. Stogin, B. T. S. Wong, *Proc. Natl. Acad. Sci. U. S. A.* **2016**, *113*, 268.
[19] G. Bodelon, V. Montes-Garcia, V. Lopez-Puente, E. H. Hill, C. Hamon, M. N. Sanz-Ortiz, S. Rodal-Cedeira, C. Costas, S. Celiksoy, I. Perez-Juste, L. Scarabelli, A. La Porta, J. Perez-Juste, I. Pastoriza-Santos, L. M. Liz-Marzan, *Nat. Mater.* **2016**, *15*, 1203.
[20] D. K. Lim, K. S. Jeon, H. M. Kim, J. M. Nam, Y. D. Suh, *Nat. Mater.* **2010**, *9*, 60.
[21] M. Yilmaz, E. Babur, M. Ozdemir, R. L. Gieseking, Y. Dede, U. Tamer, G. C. Schatz, A. Facchetti, H. Usta, G. Demirel, *Nat. Mater.* **2017**, *16*, 918.
[22] Y. C. Cao, R. Jin, C. A. Mirkin, *Science* **2002**, *297*, 1536.
[23] R. A. Alvarez-Puebla, A. Agarwal, P. Manna, B. P. Khanal, P. Aldeanueva-Potel, E. Carbó-Argibay, N. Pazos-Pérez, L. Vigderman, E. R. Zubarev, N. A. Kotov, L. M. Liz-Marzán, *Proc. Natl. Acad. Sci. U. S. A.* **2011**, *108*, 8157.
[24] Y. B. Zheng, J. L. Payton, T. B. Song, B. K. Pathem, Y. Zhao, H. Ma, Y. Yang, L. Jensen, A. K. Jen, P. S. Weiss, *Nano Lett.* **2012**, *12*, 5362.
[25] X. Gao, P. Zheng, S. Kasani, S. Wu, F. Yang, S. Lewis, S. Nayeem, E. B. Engler-Chiurazzi, J. G. Wigginton, J. W. Simpkins, N. Wu, *Anal. Chem.* **2017**, *89*, 10104.
[26] Z. L. Zhang, P. Xu, X. Z. Yang, W. J. Liang, M. T. Sun, *J. Photochem. Photobiol., C* **2016**, *27*, 100.
[27] C. Zong, M. Xu, L. J. Xu, T. Wei, X. Ma, X. S. Zheng, R. Hu, B. Ren, *Chem. Rev.* **2018**, *118*, 4946.
[28] S. S. Masango, R. A. Hackler, N. Large, A. I. Henry, M. O. McAnally, G. C. Schatz, P. C. Stair, R. P. Van Duyne, *Nano Lett.* **2016**, *16*, 4251.
[29] S. Y. Ding, J. Yi, J. F. Li, B. Ren, D. Y. Wu, R. Panneerselvam, Z. Q. Tian, *Nat. Rev. Mater.* **2016**, *1*, 16021.
[30] J. F. Li, Y. F. Huang, Y. Ding, Z. L. Yang, S. B. Li, X. S. Zhou, F. R. Fan, W. Zhang, Z. Y. Zhou, D. Y. Wu, B. Ren, Z. L. Wang, Z. Q. Tian, *Nature* **2010**, *464*, 392.
[31] Y. Fang, N.-H. Seong, D. D. Dlott, *Science* **2008**, *321*, 388.
[32] D. K. Lim, K. S. Jeon, J. H. Hwang, H. Kim, S. Kwon, Y. D. Suh, J. M. Nam, *Nat. Nanotechnol.* **2011**, *6*, 452.
[33] L. Tong, T. Zhu, Z. Liu, *Chem. Soc. Rev.* **2011**, *40*, 1296.
[34] X. Chen, N. C. Lindquist, D. J. Klemme, P. Nagpal, D. J. Norris, S. H. Oh, *Nano Lett.* **2016**, *16*, 7849.
[35] M. A. Alibakhshi, J. R. Halman, J. Wilson, A. Aksimentiev, K. A. Afonin, M. Wanunu, *ACS Nano* **2017**, *11*, 9701.
[36] H. J. Butler, L. Ashton, B. Bird, G. Cinque, K. Curtis, J. Dorney, K. Esmonde-White, N. J. Fullwood, B. Gardner, P. L. Martin-Hirsch, M. J. Walsh, M. R. McAinsh, N. Stone, F. L. Martin, *Nat. Protoc.* **2016**, *11*, 664.
[37] D. Z. Aoune Barhoumi, F. Tam, N. J. Halas, *J. Am. Chem. Soc.* **2008**, *130*, 5523.
[38] L. J. Xu, Z. C. Lei, J. Li, C. Zong, C. J. Yang, B. Ren, *J. Am. Chem. Soc.* **2015**, *137*, 5149.
[39] E. Pazos, M. Garcia-Algar, C. Penas, M. Nazarenus, A. Torruella, N. Pazos-Perez, L. Guerrini, M. E. Vazquez, E. Garcia-Rico, J. L. Mascarenas, R. A. Alvarez-Puebla, *J. Am. Chem. Soc.* **2016**, *138*, 14206.
[40] L. A. Lane, X. Qian, S. Nie, *Chem. Rev.* **2015**, *115*, 10489.
[41] Y. Wang, B. Yan, L. Chen, *Chem. Rev.* **2013**, *113*, 1391.
[42] L. Xu, H. Kuang, C. Xu, W. Ma, L. Wang, N. A. Kotov, *J. Am. Chem. Soc.* **2012**, *134*, 1699.
[43] S. Cherukulappurath, S. H. Lee, A. Campos, C. L. Haynes, S. H. Oh, *Chem. Mater.* **2014**, *26*, 2445.
[44] X. Yang, C. Gu, F. Qian, Y. Li, J. Z. Zhang, *Anal. Chem.* **2011**, *83*, 5888.
[45] P. Hermann, A. Hermelink, V. Lausch, G. Holland, L. Moller, N. Bannert, D. Naumann, *Analyst* **2011**, *136*, 1148.
[46] K. Olschewski, E. Kammer, S. Stockel, T. Bocklitz, T. Deckert-Gaudig, R. Zell, D. Cialla-May, K. Weber, V. Deckert, J. Popp, *Nanoscale* **2015**, *7*, 4545.
[47] Y. Y. Lin, J. D. Liao, M. L. Yang, C. L. Wu, *Biosens. Bioelectron.* **2012**, *35*, 447.
[48] C. W. Chang, J. D. Liao, A. L. Shiau, C. K. Yao, *Sens. Actuators, B* **2011**, *156*, 471.
[49] L. Chen, S. Xu, J. Li, *Chem. Soc. Rev.* **2011**, *40*, 2922.
[50] L. Chen, X. Wang, W. Lu, X. Wu, J. Li, *Chem. Soc. Rev.* **2016**, *45*, 2137.
[51] Z. Zhang, Y. Fu, W. Yu, X. Qin, Z. Xue, Y. Liu, D. Luo, C. Yan, X. Sun, T. Wang, *Adv. Mater.* **2016**, *28*, 9589.
[52] J. Y. Lim, J. S. Nam, S. E. Yang, H. Shin, Y. H. Jang, G. U. Bae, T. Kang, K. I. Lim, Y. Choi, *Anal. Chem.* **2015**, *87*, 11652.
[53] S. K. Yang, N. Sun, B. B. Stogin, J. Wang, Y. Huang, T. S. Wong, *Nat. Commun.* **2017**, *8*, 1285.
[54] N. Vogel, C. K. Weiss, K. Landfester, *Soft Matter* **2012**, *8*, 4044.
[55] X. G. Zhang, Z. G. Dai, S. Y. Si, X. L. Zhang, W. Wu, H. B. Deng, F. B. Wang, X. H. Xiao, C. Z. Jiang, *Small* **2017**, *13*, 1603347.
[56] X. G. Zhang, S. Y. Si, X. L. Zhang, W. Wu, X. H. Xiao, C. Z. Jiang, *ACS Appl. Mater. Interfaces* **2017**, *9*, 40726.
[57] Z. G. Dai, X. H. Xiao, W. Wu, Y. P. Zhang, L. Liao, S. S. Guo, J. J. Ying, C. X. Shan, M. T. Sun, C. Z. Jiang, *Light: Sci. Appl.* **2015**, *4*, e342.
[58] S. Y. Si, W. Q. Li, X. L. Zhao, M. Han, Y. N. Yue, W. Wu, S. S. Guo, X. G. Zhang, Z. G. Dai, X. W. Wang, X. H. Xiao, C. Z. Jiang, *Adv. Mater.* **2017**, *29*, 1604623.
[59] R. R. Dourmashkin, S. A. McCall, N. Dourmashkin, M. J. Hannah, *F1000Research* **2018**, *7*, 302.

© 2019 WILEY-VCH Verlag GmbH & Co. KGaA, Weinheim